

A Unified Methodology for Calculation of Compliance and Stiffness Contribution Tensors of Inhomogeneities of Arbitrary 2D and 3D Shapes Embedded in Isotropic Matrix – Open Access Software.

Abstract.

Property contribution tensors constitute basic building blocks for evaluation of effective properties of heterogeneous materials. Most of the existing results, however, are obtained for inhomogeneities of simple shapes, like ellipsoidal. With this paper we introduce open access software that allows one to calculate the components of compliance and stiffness contribution tensors of inhomogeneities of any shape. The software uses mesh free method based on a class of Gaussian approximating functions. Here we present details of the method and illustrate it by several examples. The software can be downloaded from the website of NMSU Center for Micromechanics <https://centerformichromechanics.nmsu.edu>.

1. Introduction.

Compliance and stiffness contribution tensors are used in micromechanics for quantitative characterization of the effect of individual inhomogeneities on the overall elastic properties. Compliance contribution tensor has been first introduced in the context of ellipsoidal pores and cracks by Horii and Nemat-Nasser [1] (see also detailed discussion in the book of Nemat-Nasser and Hori [2]) who also explicitly expressed its components in terms of Eshelby tensor. Kachanov et al [3] calculated this tensor for a variety of non-elliptical 2D shapes using method of conformal mappings. For general case of ellipsoidal inhomogeneities in an isotropic media, these tensors were calculated by Sevostianov and Kachanov [4], [5]. Sevostianov et al. [6] calculated components of this tensor for a spheroidal inhomogeneity embedded in a transversely isotropic material. Kushch and Sevostianov [7] established the link between compliance contribution tensor and dipole moments. These results are obtained for ellipsoidal inhomogeneities in terms of Eshelby tensor (Eshelby [8], [9]; Mura [10]). We have to point out, however, that, for non-ellipsoidal inhomogeneities, this link is lost. Eshelby tensor is irrelevant for the problem of effective properties of heterogeneous material with non-ellipsoidal inhomogeneities, and compliance contribution tensor, therefore, has to be calculated independently.

While for non-elliptical inhomogeneities in 2D settings many analytical and numerical results have been obtained by conformal mapping (see Zimmerman [11]; Kachanov et al. [3]; Jasiuk et al. [12]; Tsukrov and Novak [13], [14]; Ekneligoda and Zimmerman [15], [16]), only a limited number of numerical results and approximate estimates are available for non-ellipsoidal 3D shapes. In 3D, the problem of the elastic fields associated with an inhomogeneity of “irregular” (non-ellipsoidal) shape reduces to an integral equations and generally requires computational approaches (although, in some cases, solution can be obtained in the form of infinite series, see results of Argatov and Sevostianov [17] and Krasnitskii et al. [18] for thin and regular rigid toroids).

Compliance contribution tensors for several examples of pores of irregular shape typical for carbon-carbon composites have been calculated by Drach et al. [19] using FEM. The authors give the values of the components of compliance contribution tensors for several specific shapes (Tables 1 and 2 in their paper), but did not discuss effect of any particular irregularity factor. Compliance contribution tensors of concave pores of various shape have been calculated by Sevostianov et al. [20], Sevostianov and Giraud [21], Chen et al. [22], Sevostianov et al. [23], Chen et al. [24], Trofimov et al. [25] and Markov et al. [26]. Stiffness contribution tensors have been evaluated for particles of various polyhedral shape by Trofimov et al. [27]; for helical fibers – by Trofimov and Sevostianov [28] and Trofimov et al. [29].

In the narrower context of irregularly shaped cracks, certain results were obtained for compliance contribution tensors by Fabrikant [30], Sevostianov and Kachanov [5] (planar cracks of non-elliptical shape), Grechka et al. [31] (intersecting planar cracks), Mear et al. [32] (non-planar cracks), and Kachanov and Sevostianov [33] (2012) (cracks growing from pores); Trofimov et al. [34], Markov et al. [35], Markov et al. [36] (various configurations of planar and non-planar cracks with islands of contact).

Rasool and Böhm [37] and Böhm and Rasool [38] analyzed shape effects on the effective elastic and thermal properties of the composites containing randomly oriented and distributed spherical, octahedral, cubical and tetrahedral particles. Drach et al. [39] proposed to evaluate effect of pores of irregular shape on the overall elastic moduli using pore projected areas. This approach works well for prediction of the overall Young’s moduli in different directions. Drach et al. [40] performed a comprehensive numerical analysis of the pore shape on the overall properties of solids with porosity levels up to 25%. An alternative approach consists of direct

computation of stress and strain fields for a given (deterministic) microstructure by discretizing the domain and using the FEM, and then post-processing the averages of the stress and strain fields (see, for example, Roberts and Garboczi [41], [42]; Arns et al. [43]; Garboczi and Douglas [44]).

The problem faced by the currently available computational tools is that they are generally not all openly available and, more importantly, there is no general software package comprising all software packages necessary to calculate contributions of the inhomogeneities into overall elastic properties. At last, the available tools do not have the accuracy and the functionalities needed to calculate property contribution tensors, required by the homogenization methods. Consequently, newcomers must spend much time to get used to the problem, handle incompatibilities of definitions, and gather different tools to achieve each task. As a result, each team working in the area of micromechanics has developed its own tools. This has scattered the efforts instead of focusing them on the development of generic software suited for everyone.

With this paper, we introduce a new open access software package named AMAT that implements the mesh free numerical method based on a class of Gaussian approximating functions. The theory of approximation by these functions was developed by Maz'ya and Schmidt [45]. The problem is formulated in terms of integral equations for stress or strain fields in the case of 3D inhomogeneities (Kanaun [46]) or displacement discontinuity in the case of 2D ones (cracks) (Kanaun [47]). For discretization of these equations, a class of Gaussian approximating functions centered at the nodes of regular node grids is used; thus, the system of linear equations is formed in a very efficient way (Kanaun and Markov [48]). It should be noted that although commercial FEM-based software (see, e.g., Babaii [49]) present certain advantages, as well-tested solvers and graphical post-processors; this type of software is not well-suited for the modeling of infinite media and 2D shapes (see, e.g., Trofimov et al. [25]).

The paper is structured as follows: in Section 2, we follow Kachanov and Sevostianov [50] and define compliance and stiffness contribution tensors for an inhomogeneity. Section 3 focuses on the computational method used for evaluation of these tensors. In Section 4, we explain how the software can be run. Section 5 contains several examples of the calculations. We first start, of course, with the example of a spheroid, for which the exact result can be expressed in elementary functions. Then we discuss more complex shapes.

2. Background material: property contribution tensors.

In the context of the elastic properties, the average, over a representative volume element (RVE) V strain can be represented as a sum

$$\boldsymbol{\varepsilon} = \mathbf{S}^0 : \boldsymbol{\sigma}^0 + \Delta \boldsymbol{\varepsilon}, \quad (2.1)$$

where \mathbf{S}^0 is the compliance tensor of the matrix and $\boldsymbol{\sigma}^0$ represents the uniform boundary conditions (Hill [51], Hashin [52]): tractions on ∂V have the form $\mathbf{t}|_{\partial V} = \boldsymbol{\sigma}^0 \cdot \mathbf{n}$ where $\boldsymbol{\sigma}^0$ is a constant tensor; $\boldsymbol{\sigma}^0$ is also called “far-field”, or “remotely applied”, stress; in absence of inhomogeneities, it would have been uniform in V . The material is assumed to be linear elastic, hence the extra (average over V) strain due to some inhomogeneity that occupies volume V_1 is a linear function of applied stress:

$$\Delta \boldsymbol{\varepsilon} = \frac{V_1}{V} \mathbf{H} : \boldsymbol{\sigma}^0, \quad (2.2)$$

where \mathbf{H} is a fourth-rank *compliance contribution tensor* of the inhomogeneity. In the case of multiple inhomogeneities, the extra compliance due to their presence is given by

$$\Delta \mathbf{S} = \frac{1}{V} \sum V^{(k)} \mathbf{H}^{(k)}, \quad (2.3)$$

Alternatively, one can consider the extra average (over V) stress $\Delta \boldsymbol{\sigma}$ due to an inhomogeneity under uniform displacement boundary conditions (displacements on ∂V have the form $\mathbf{u}|_{\partial V} = \boldsymbol{\varepsilon}^0 \cdot \mathbf{n}$ where $\boldsymbol{\varepsilon}^0$ is a constant tensor). This defines the *stiffness contribution tensor* \mathbf{N} of an inhomogeneity:

$$\Delta \boldsymbol{\sigma} = \frac{V_1}{V} \mathbf{N} : \boldsymbol{\varepsilon}^0, \quad (2.4)$$

In the case of multiple inhomogeneities, the extra stiffness due to inhomogeneities is given by

$$\Delta \mathbf{C} = \frac{1}{V} \sum V^{(k)} \mathbf{N}^{(k)}. \quad (2.5)$$

The \mathbf{H} and \mathbf{N} tensors are determined by the shape of the inhomogeneity and are independent of its size; they also depend on elastic constants of the matrix and the inhomogeneity. In the framework of the developed software, the \mathbf{N} tensor is calculated from the average stress $\langle \sigma_{ij} \rangle_m$ inside the inhomogeneity:

$$N_{ijkl}(\varepsilon_{kl}^0)_m = (\sigma_{ij}^0)_m - \langle \sigma_{ij} \rangle_m, \quad (2.6)$$

where $(\varepsilon_{kl}^0)_m$ and $(\sigma_{ij}^0)_m$ are prescribed components of strain and stress correspondingly; a total amount of six load cases m is considered: three simple tensile and three simple shear loads in the main directions. Similarly, the \mathbf{H} tensor may be found from the average strain $\langle \varepsilon_{ij} \rangle_m$ inside the inhomogeneity:

$$H_{ijkl}(\sigma_{kl}^0)_m = (\varepsilon_{ij}^0)_m - \langle \varepsilon_{ij} \rangle_m. \quad (2.7)$$

Formulas (2.3) and (2.5) highlight the fundamental importance of \mathbf{H} and \mathbf{N} tensors: it is *them* that have to be summed up (or averaged over orientations), in the context of the effective elastic properties. The sums properly reflect compliance contributions of individual inhomogeneities. In certain cases, a simple geometrical factor (such as volume fraction c , crack density ρ , or, in more complex cases, certain average shape factor, see Section 6) can be taken out of the mentioned sums as a multiplier. However, as a rule, this cannot be done for mixtures of diverse shapes.

In the case of identical shapes,

$$\Delta \mathbf{S} = c\mathbf{H}, \quad \Delta \mathbf{C} = c\mathbf{N}. \quad (2.8)$$

Here $c = \frac{V_1}{V}$, as the volume V_1 of all the inhomogeneities is the same.

The \mathbf{H} and \mathbf{N} tensors of an inhomogeneity are, obviously, interrelated. The overall compliance tensor of a representative volume containing one inhomogeneity $\mathbf{S}^0 + (V_1/V)\mathbf{H}$ is an inverse of its stiffness tensor $\mathbf{C}^0 + (V_1/V)\mathbf{N}$, i.e. their product equals the fourth-rank unit tensor

implying that $\mathbf{N} = -\mathbf{C}^0 : \mathbf{H} : \mathbf{C}^0 - (V_1/V) \mathbf{N} : \mathbf{H} : \mathbf{C}^0$. Since the ratio (V_1/V) can be made arbitrarily small by enlarging V , the second term can be neglected so that:

$$\mathbf{N} = -\mathbf{C}^0 : \mathbf{H} : \mathbf{C}^0 \quad (2.9)$$

In the case of an isotropic matrix,

$$-N_{ijkl} = \lambda_0^2 H_{mnmnr} \delta_{ij} \delta_{kl} + \mu_0^2 H_{ijkl} + \lambda_0 \mu_0 (\delta_{ij} H_{mmkl} + \delta_{kl} H_{mmij}) \quad (2.10)$$

where λ_0 and μ_0 are Lamé constants of the matrix.

3. Methods of calculations.

In order to calculate numerically the compliance and stiffness contribution tensors \mathbf{H} and \mathbf{N} for virtually any finite inhomogeneity shape, we consider the mesh free method based on a class of Gaussian approximating functions. For the sake of efficiency, we use two different algorithms for 3D shapes (solid inclusions and pores) and 2D ones (planar cracks).

3.1. Solid inclusions and pores.

Let us formulate the problem in terms of integral equations for strain $\boldsymbol{\varepsilon}(x)$ and stress $\boldsymbol{\sigma}(x)$ fields inside a inhomogeneity that occupies the finite volume V_1 in an infinite elastic medium (see, e.g., Kanaun and Levin [53]):

$$\boldsymbol{\varepsilon}_{ij}(x) + \int_{V_1} \mathbf{K}_{ijkl}(x-x') \mathbf{C}_{klmn}^{10}(x') \boldsymbol{\varepsilon}_{mn}(x') dx' = \boldsymbol{\varepsilon}_{ij}^0(x), \quad (3.1)$$

$$\boldsymbol{\sigma}_{ij}(x) - \int_{V_1} \mathbf{S}_{ijkl}(x-x') \mathbf{S}_{klmn}^{10}(x') \boldsymbol{\sigma}_{mn}(x') dx' = \boldsymbol{\sigma}_{ij}^0(x), \quad (3.2)$$

where $\mathbf{C}^{10}(x) = \mathbf{C}^1 - \mathbf{C}^0$, $x \in V_1$; $\mathbf{C}^{10}(x) = 0$, $x \notin V_1$. Similarly, $\mathbf{S}^{10}(x) = \mathbf{S}^1 - \mathbf{S}^0$, $x \in V_1$; $\mathbf{S}^{10}(x) = 0$, $x \notin V_1$. The kernels $\mathbf{K}(x)$ and $\mathbf{S}(x)$ are calculated from the second derivative of the Green function $\mathbf{G}(x)$ of the matrix:

$$K_{ijkl}(x) = -\left[\partial_i \partial_k G_{jl}(x) \right]_{(ij)(kl)}, \quad (3.3)$$

$$S_{ijkl}(x) = C_{ijmn}^0 K_{mnpq}(x) C_{pqkl}^0 - C_{ijkl}^0 \delta(x), \quad (3.4)$$

where $\delta(x)$ is Dirac's delta function; indices in parenthesis mean symmetrization. The properties of these kernels were studied in detail by Kanaun [54] and Kunin [55].

For the discretization of the integral equations given in (3.1) and (3.2), we take the approximate solutions in the following forms:

$$\varepsilon_{ij}(x) \approx \sum_{s=1}^N \varepsilon_{ij}^{(s)} \varphi(x - x^{(s)}), \quad (3.5)$$

$$\sigma_{ij}(x) \approx \sum_{s=1}^N \sigma_{ij}^{(s)} \varphi(x - x^{(s)}), \quad (3.6)$$

where $\varepsilon^{(s)}$ and $\sigma^{(s)}$ are unknown values of strain and stress at the node $x^{(s)}$ ($s=1,2,\dots,N$) of a regular grid that covers a cuboid W that contains the region V_1 occupied by the inhomogeneity, N is the total number of the nodes in W (Figure 1).

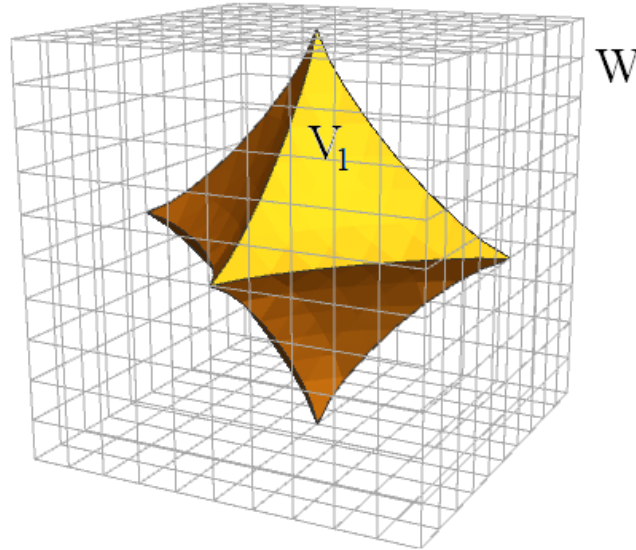


Figure 1. An example of a volume W of a medium covered by a regular grid of nodes containing an inhomogeneity occupying a volume V_1 .

The function $\varphi(x)$ is the 3D-Gaussian distribution function:

$$\varphi(x) = \frac{1}{(\pi H)^{3/2}} \exp\left(-\frac{|x|^2}{Hh^2}\right), \quad (3.7)$$

where h is the grid step, H is a non-dimensional parameter of the order 1. For reliable approximations, the condition $h/L > \exp(-\pi^2 H)$, where L is the characteristic size of the inhomogeneity, should be kept (Maz'ya and Schmidt [45]); at the same time, H cannot be higher than $O(1)$, as this will result in very low values of $\varphi(x)$. Previous experiments have shown that the optimal value of $H = 2$.

After substituting the solutions (3.5) and (3.6) into the integral equations (3.1) and (3.2), correspondingly, we obtain the following systems of linear equations:

$$\mathcal{E}_{ij}^{(r)} + \sum_{s=1}^N \Pi_{ijkl}^{(r,s)} C_{klmn}^{10(s)} \mathcal{E}_{mn}^{(s)} = \mathcal{E}_{ij}^{0(r)}, \quad r = 1, \dots, N, \quad (3.8)$$

$$\Pi_{ijkl}^{(r,s)} = \Pi_{ijkl} \left(x^{(r)} - x^{(s)} \right), \quad C_{ijkl}^{10(s)} = C_{ijkl}^{10} \left(x^{(s)} \right), \quad \mathcal{E}_{ij}^{0(s)} = \mathcal{E}_{ij}^0 \left(x^{(s)} \right), \quad (3.9)$$

$$\sigma_{ij}^{(r)} + \sum_{s=1}^N \Gamma_{ijkl}^{(r,s)} S_{klmn}^{10(s)} \sigma_{mn}^{(s)} = \sigma_{ij}^{0(r)}, \quad r = 1, \dots, N, \quad (3.10)$$

$$\Gamma_{ijkl}^{(r,s)} = \Gamma_{ijkl} \left(x^{(r)} - x^{(s)} \right), \quad S_{ijkl}^{10(s)} = S_{ijkl}^{10} \left(x^{(s)} \right), \quad \sigma_{ij}^{0(s)} = \sigma_{ij}^0 \left(x^{(s)} \right). \quad (3.11)$$

The integral operators $\Pi(x)$ and $\Gamma(x)$ are calculated over the entire 3D space R ; this is possible due to the fact that Gaussian functions decrease very fast.

$$\Pi_{ijkl}(x) = \int_R K_{ijkl}(x-x') \varphi(x') dx', \quad (3.12)$$

$$\Gamma_{ijkl}(x) = \int_R S_{ijkl}(x-x') \varphi(x') dx'. \quad (3.13)$$

These integrals are calculated explicitly (see, e.g., Kanaun and Pervago [56]). Also, the left-hand side matrices of the systems of linear equations (3.8) and (3.10) have Toeplitz's structure;

as a result, only one row and one column must be stored in computer memory. For the numerical solution of these systems, Biconjugate Gradient Stabilized Method (BiCGStab) is used. For the calculation of matrix-vector products required at every iteration of BiCGStab, the fast Fourier transform technique is applied (see Kanaun [46]). Note that for the inclusions the Young's modulus of which is smaller than the Young's modulus of the matrix, the equation (3.8) for strains converges faster than the one for stresses (3.10), and vice versa (Kanaun and Pervago [56]).

Once either of the systems (3.8) and (3.10) is solved, the compliance and stiffness contribution tensors \mathbf{H} and \mathbf{N} are calculated by the procedure described in Section 2 (see (2.6) and (2.7)). The average stress $\langle \sigma_{ij} \rangle_m$ or strain $\langle \varepsilon_{ij} \rangle_m$ inside the inhomogeneity is calculated numerically as the volumetric average of the stress $\sigma_{ij}^{(s)}$ and strain $\varepsilon_{ij}^{(s)}$ at the nodes $x^{(s)} \in V_1$.

3.2. Planar cracks.

Let us consider an isolated planar crack with surface Ω and unit normal \mathbf{n} subjected to an external stress $\boldsymbol{\sigma}^0(x)$; $\mathbf{b}(x) = \mathbf{u}^+ - \mathbf{u}^-$ is the displacement discontinuity vector on Ω (crack opening). The stress field at Ω can be expressed in the form similar to (3.2) (Kanaun et al. [57])

$$\sigma_{ij}(x) = \sigma_{ij}^0(x) + \int_{\Omega} S_{ijkl}(x-x') n_k b_l(x') dx'. \quad (3.14)$$

Since crack faces are traction free, the following boundary condition must be satisfied:

$$n_i \sigma_{ij}(x) \Big|_{\Omega} = 0. \quad (3.15)$$

The integral equation for the crack opening $b_i(x)$ follows from Eqs. (2.1) and (2.4):

$$\int_{\Omega} n_k S_{kijl}(x-x') n_l b_j(x') d\Omega' = -n_j \sigma_{ji}^0(x), \quad (3.16)$$

In order to convert the integral equation (3.16) to a system of linear algebraic equations, a technique similar to the one developed for 3D inhomogeneities is used. We cover the planar rectangular area $\bar{\Omega}$ that envelops the crack surface Ω by a regular grid $x^{(s)}$ of N nodes, as shown in Figure 2.

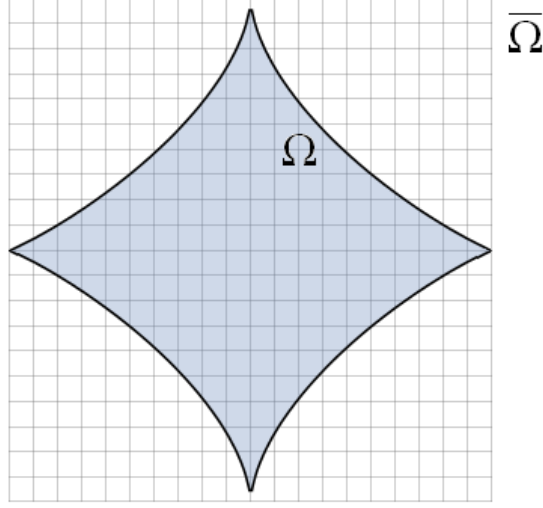


Figure 2. A rectangular area $\bar{\Omega}$ covered by a regular grid of nodes enveloping a planar crack with surface Ω .

As in the previous Subsection, for the discretization of the integral equation (3.16), we use Gaussian approximating functions centered at the node set $x^{(s)}$:

$$b_i(x) \approx \sum_{s=1}^N b_i^{(s)} \varphi(x - x^{(s)}) \quad (3.17)$$

Here $\mathbf{b}^{(s)}$ are constant vectors (displacement discontinuities at the nodes); for the nodes lying outside Ω , $\mathbf{b}^{(s)} = 0$; $\varphi(x - x^{(s)})$ is the 2D Gaussian function:

$$\varphi(x) = \frac{1}{\pi H} \exp\left(-\frac{x_1^2 + x_2^2}{Hh^2}\right). \quad (3.18)$$

Thus, we obtain a system of linear algebraic equations for components of the vector $\mathbf{b}^{(s)}$:

$$\sum_{s=1}^N I_{ij}^{(p,s)} b_j^{(s)} = t_i^{0(p)}, \quad p = 1, 2, \dots, N, \quad (3.19)$$

$$I_{ij}^{(p,s)} = I_{ij}(x^{(p)} - x^{(s)}), \quad t_i^{0(p)} = -n_j \sigma_{ji}^0(x^{(p)}). \quad (3.20)$$

The integral operator $\mathbf{I}(x)$ is calculated over the entire 2D plane P :

$$I_{ij}(x) = \int_P n_k S_{kijl}(x - x') n_l \varphi(x') dx'. \quad (3.21)$$

As in the case of the integrals (3.12) and (3.13), the integral (3.21) can be calculated explicitly (see Kanaun [47]). The solution procedure for the system of equations (3.19) is the

same as in the case of 3D inhomogeneities. For a crack of arbitrary shape, the tensor \mathbf{H} may be related to the calculated crack opening displacement as

$$\frac{V_1}{V} H_{ijkl} \sigma_{kl}^0 = \frac{1}{2V} \int_{\Omega} [n_i b_j(x) + n_j b_i(x)] d\Omega . \quad (3.22)$$

Similarly to the case of 3D inhomogeneities, the integral in (3.22) is calculated numerically for the nodes $x^{(s)} \in \Omega$.

4. Running the code.

The main novelty of the current work is the introduction of a user-friendly interface that allows one to apply the described numerical method in a simple and intuitive way; screenshots of the interface are shown in Figures 3 and 4. In the current state, the developed software allows one to calculate the compliance and stiffness contribution tensors \mathbf{H} and \mathbf{N} of an inhomogeneity of any of the three types: solid inclusion (default), pore, and crack. The interface presents corresponding checkboxes for the latter two cases (Figure 3). Currently, both the matrix and the solid inclusions are taken as isotropic only (the fields other than ‘E1’ and ‘v12’ are not active). The user may enter the inhomogeneity shape in two ways: by manually typing the equation that describes the shape or by importing a stereolithography (.stl) file.

Matrix elastic constants

E1	E2	E3
1		
v12	v23	v31
0.3		
G12	G23	G31

Inhomogeneity elastic constants

E1	E2	E3
10		
v12	v23	v31
0.25		
G12	G23	G31

Pore

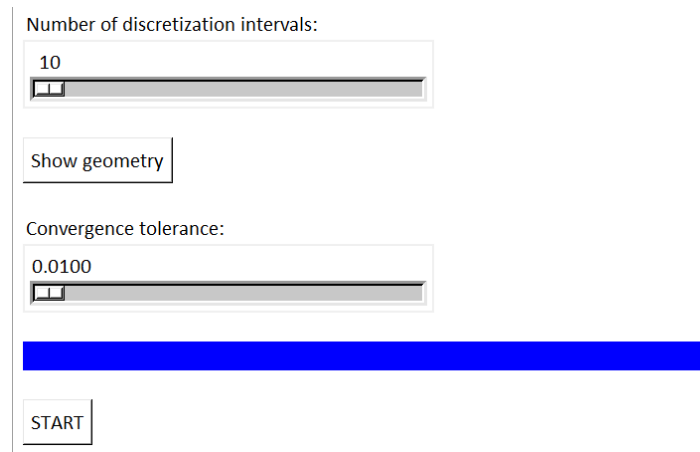
Crack

Function Import .STL:

`x**2+y**2+z**2-1` =0

Figure 3. Part of the interface of AMAT software dedicated to the shape input with some sample values corresponding to a spherical inclusion.

In order to improve the precision of the calculations, the user may increase the number of discretization intervals, thus, adding grid nodes. It should be noted that very high number of discretization intervals in the case of 3D shapes may result in a long calculation time or even a random access memory (RAM) overflow. It is possible to visualize the inhomogeneity and the node grid that covers it. The convergence tolerance slider defines the convergence criterion for the numerical solution of the system of linear equations: (3.8), (3.10), and (3.19), depending on the case; lower values may improve the calculation precision.



The image shows a software interface for adjusting precision. It features two sliders: the top one is labeled 'Number of discretization intervals:' and is set to '10'; the bottom one is labeled 'Convergence tolerance:' and is set to '0.0100'. Below the sliders is a 'Show geometry' button, a thick blue horizontal bar, and a 'START' button.

Figure 4. Part of the interface of AMAT software dedicated to the precision adjustment.

The output of the software consists of the \mathbf{H} and \mathbf{N} tensors of the considered inhomogeneity given in Voigt notation, i.e., as 6×6 matrices (Figure 5). Optionally, the detailed calculation results may be exported as a text (.txt) file.

7% Stiffness Contribution tensor N					-	□	×
2.4024	0.7673	0.6811	0.0000	0.0000	0.0000		
0.7673	2.4024	0.6811	0.0000	0.0000	0.0000		
0.6811	0.6811	1.6027	0.0000	0.0000	0.0000		
0.0000	0.0000	0.0000	0.8170	0.0000	0.0000		
0.0000	0.0000	0.0000	0.0000	0.5695	0.0000		
0.0000	0.0000	0.0000	0.0000	0.0000	0.5695		
7% Compliance Contribution tensor H					-	□	×
-2.0164	0.7469	0.5471	0.0000	0.0000	0.0000		
0.7469	-2.0164	0.5471	0.0000	0.0000	0.0000		
0.5471	0.5471	-1.3559	0.0000	0.0000	0.0000		
0.0000	0.0000	0.0000	-5.5229	0.0000	0.0000		
0.0000	0.0000	0.0000	0.0000	-3.8501	0.0000		
0.0000	0.0000	0.0000	0.0000	0.0000	-3.8501		

Figure 5. An example of the output of AMAT software for an oblate spheroidal inclusion.

5. Code validation.

In order to test the precision and efficiency of the developed software, we have applied it to the solution of several well-known problems that either have an explicit analytical solution or were solved previously by other numerical methods. The calculations were performed on a middle-level Dell Inspiron™ laptop (Intel® Core™ i7-7500U, 8 GB RAM); a user of a more advanced computer may expect a considerably better performance.

5.1. Spheroidal pores and rigid inclusions.

In the first validation case, we consider the well-known problem of a spheroidal inhomogeneity (solve analytically by Eshelby [8]) defined as:

$$\frac{x_1^2}{a^2} + \frac{x_2^2}{a^2} + \frac{x_3^2}{a_3^2} = 1, \quad (4.1)$$

where a and a_3 are the semi-axes of the spheroid if x_3 is the axis of symmetry.

We computed the property contribution tensors for the two most extreme cases of properties contrasts: rigid inclusion (with the Young's modulus of 1000 GPa) and pore (a special case; the Young's modulus contrast is 0.001 with respect to the matrix', the Poisson's ratio is 0.001). The Young's modulus of the matrix was assumed to be 1 GPa. Note that the results may be easily

scaled to any realistic value multiplying the obtained property contribution tensors by the desired Young's modulus provided that the Poisson's ratio is the same. For the current computations, the Poisson's ratio of the matrix and the rigid inclusions was equal to 0.3. In both cases, we have considered oblate ($a > a_3$) and prolate ($a < a_3$) spheroids (Figure 6).

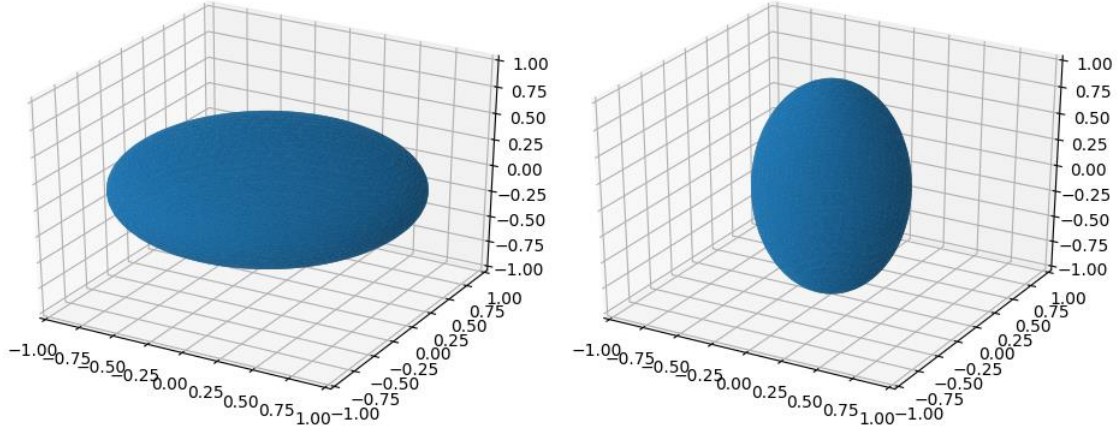


Figure 6. Oblate (left) and prolate (right) spheroidal inhomogeneities visualized by AMAT software.

The number of discretization intervals M on the side of the volume W was assumed to be 40 and 80 for the sphere which is the limiting case of spheroid. When the spheroidal inhomogeneity became more oblate/prolate, the number M was increased to maintain the total number of nodes covering the inhomogeneity constant. The calculation results are given in Figures 7 and 8. Since the resulting compliance and stiffness contribution tensors are transversally isotropic, only five independent non-zero components of contribution tensors are given in Figure 7 and 8, namely 1111, 3333, 1122, 1133, and 1212. Here the ratio $\beta = a_3/a$ for oblate spheroids and $\beta = a/a_3$ for prolate ones.

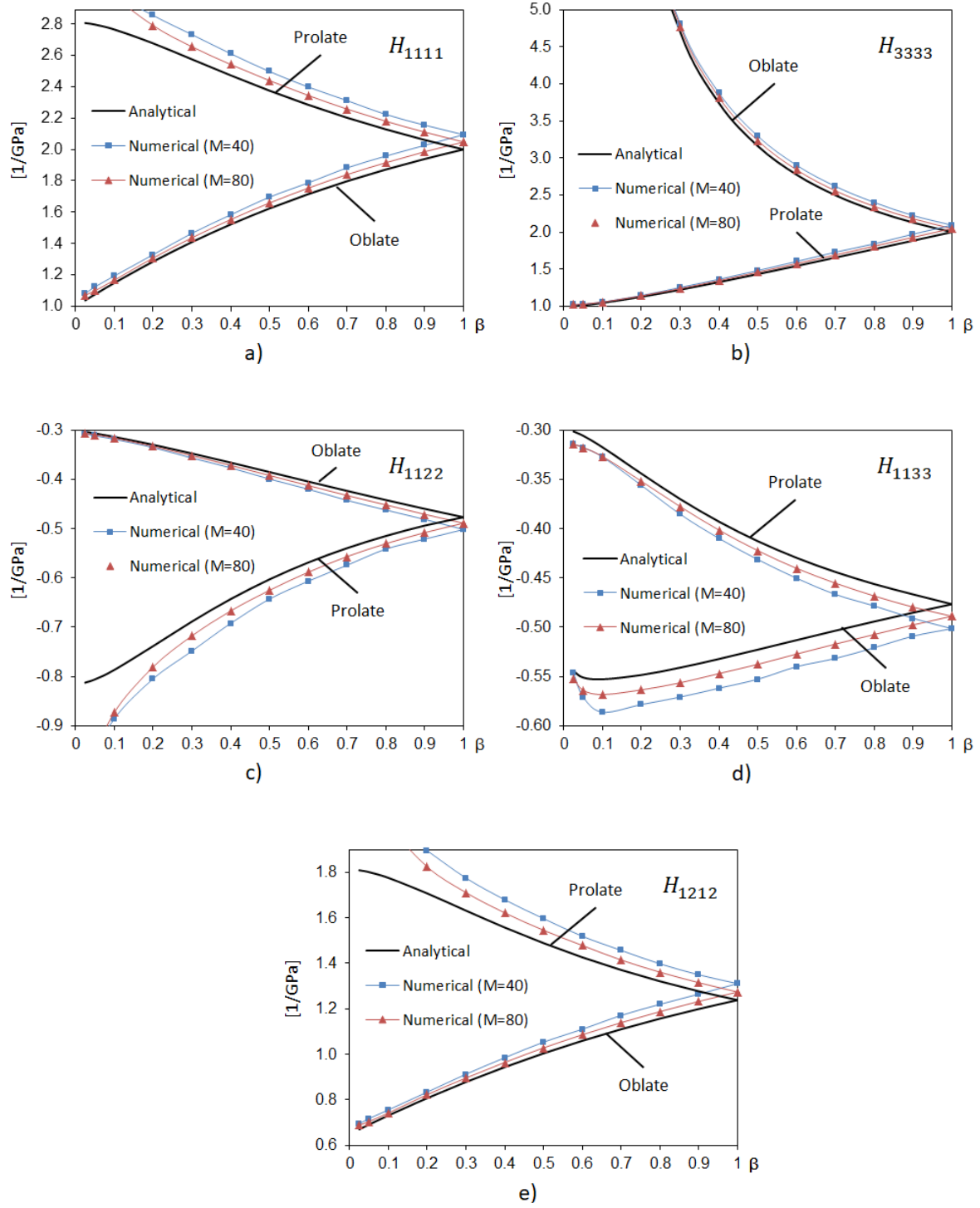


Figure 7. Components of the compliance contribution tensor of an oblate/prolate pore a) H_{1111} , b) H_{3333} , c) H_{1122} , d) H_{1133} , e) H_{1212} as functions of the ratio β .

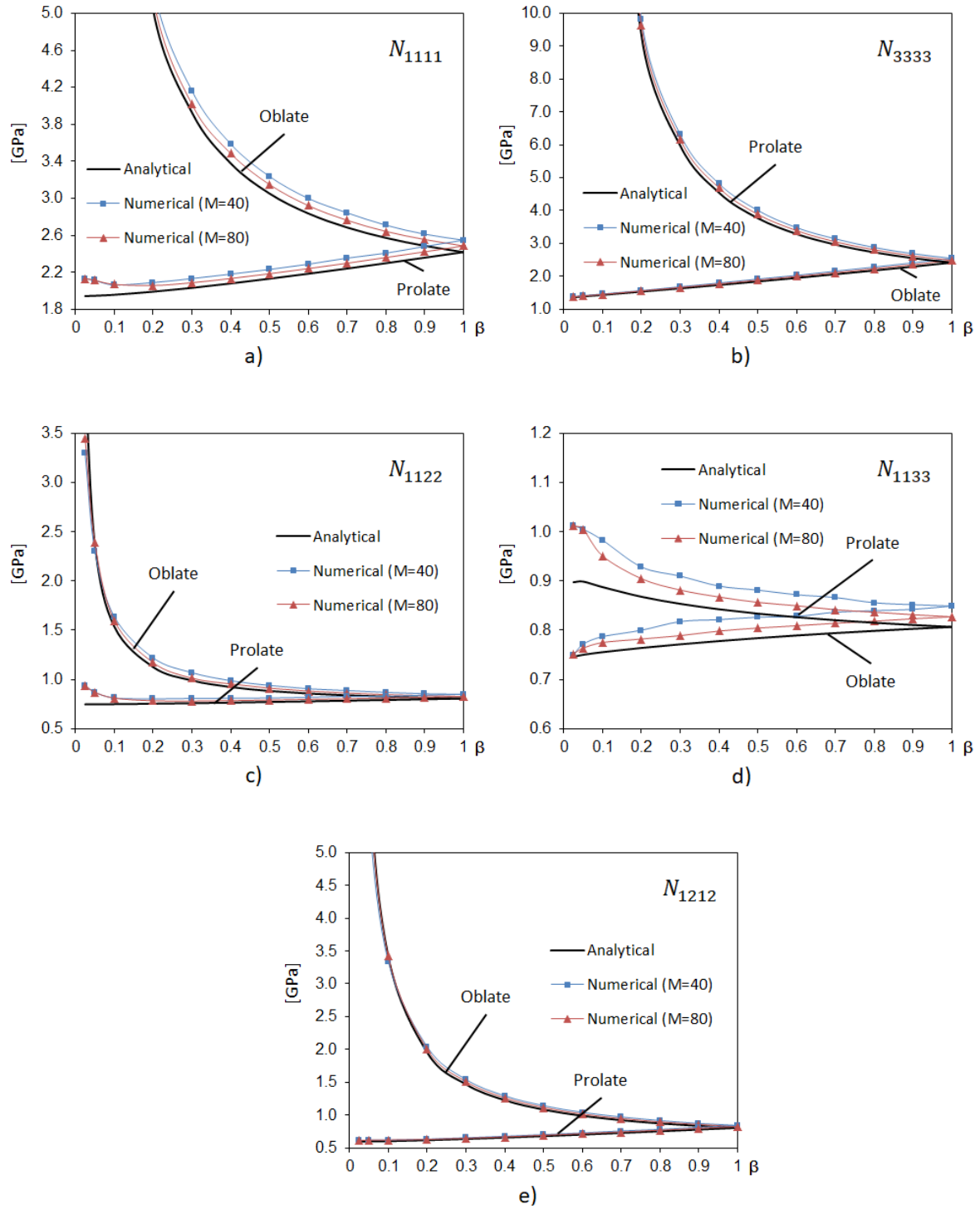


Figure 8. Components of the stiffness contribution tensor of an oblate/prolate rigid inclusion a) N_{1111} , b) N_{3333} , c) N_{1122} , d) N_{1133} , e) N_{1212} as functions of the ratio β .

It may be noted that in the case of $M = 80$ the difference between the analytical and numerical solutions does not exceed 2% for the majority of cases, with the exception of extreme cases when $\beta < 0.1$. The calculation CPU time was about 40 minutes. For $M = 40$ the accuracy of the results is still acceptable, as it does not exceed 5% for most cases; however, the calculation time decreased to about 10 minutes. Also, we should note that the results for very oblate pores ($\beta < 0.05$) are very close to the results obtained for a penny-shaped crack.

5.2. Elliptical cracks.

The next validation case involves another well-known problem of an elliptical crack (see, e.g., Kanaun and Levin [53]), the surface of which (Figure 9) is defined as

$$\frac{x_1^2}{a_1^2} + \frac{x_2^2}{a_2^2} = 1, \quad (4.2)$$

where a_1 and a_2 are the semi-axes of the ellipse; $a_1 \geq a_2$.

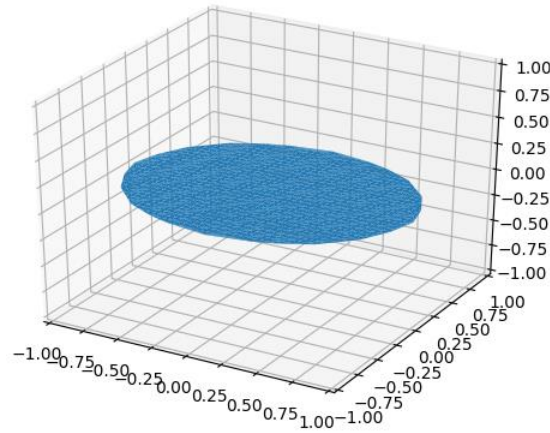


Figure 9. Elliptical crack visualized by AMAT software.

Similarly to the previous problem, the Young's modulus of the matrix was assumed to be 1 GPa and the Poisson's ratio was 0.3. For this problem, only the components 1133, 2233, and 3333 of the compliance contribution tensor are independent and are non-zero. The number M of discretization intervals was equal to 200 due to the fact that the planar crack problem is two-dimensional and, thus, the solution is much faster. The calculation results are given in Figure 10 where $\beta = a_2/a_1$.

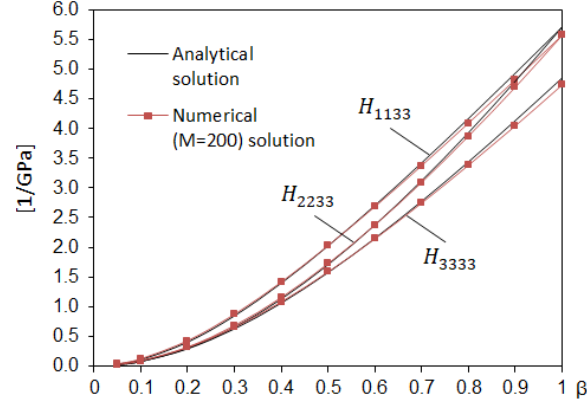


Figure 10. Components H_{1133} , H_{2233} , and H_{3333} of the compliance contribution tensor of an elliptical crack as functions of the ratio β .

The comparison of the numerical and analytical solutions has shown that the difference between them does not exceed 2.5% for the absolute majority of cases, with the exception of extremely narrow cracks ($\beta < 0.1$). The calculation CPU time was around 8 seconds.

5.3. Rigid toroidal inclusions.

In the next validation step, we considered the toroidal rigid inhomogeneity which has a more complex shape as compared to the spheroid. The analytical results for the property contribution tensors were obtained by Krasnitskii et. al. [18]. The surface of toroid (Figure 11) is described by the following equation:

$$\left(x_1^2 + x_2^2 + x_3^2 + R^2 - a^2\right)^2 - 4R^2\left(x_1^2 + x_2^2\right) = 0, \quad (4.3)$$

where R is the distance from the center of the torus to the center of the tube, and a is the radius of the tube.

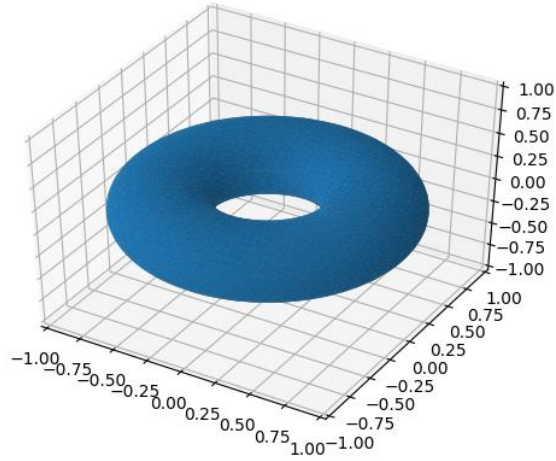


Figure 11. Torus visualized by AMAT software.

The results are obtained by considering the Young's modulus of the matrix was equal to 1 GPa that corresponds to the normalized results of Krasnitskii et. al. [18] and the Poisson's ratio was equal to 0.3. As the resulting stiffness contribution tensor is transversally isotropic, only the non-zero and independent components are given, namely 1111, 3333, 1122, 1133, and 1212. The number M of discretization intervals on the side of the volume W was taken equal to 40 and 80. The comparison of the predictions obtained by the AMAT software with the analytical results given is shown in Figure 12 where $\beta = a/R$.

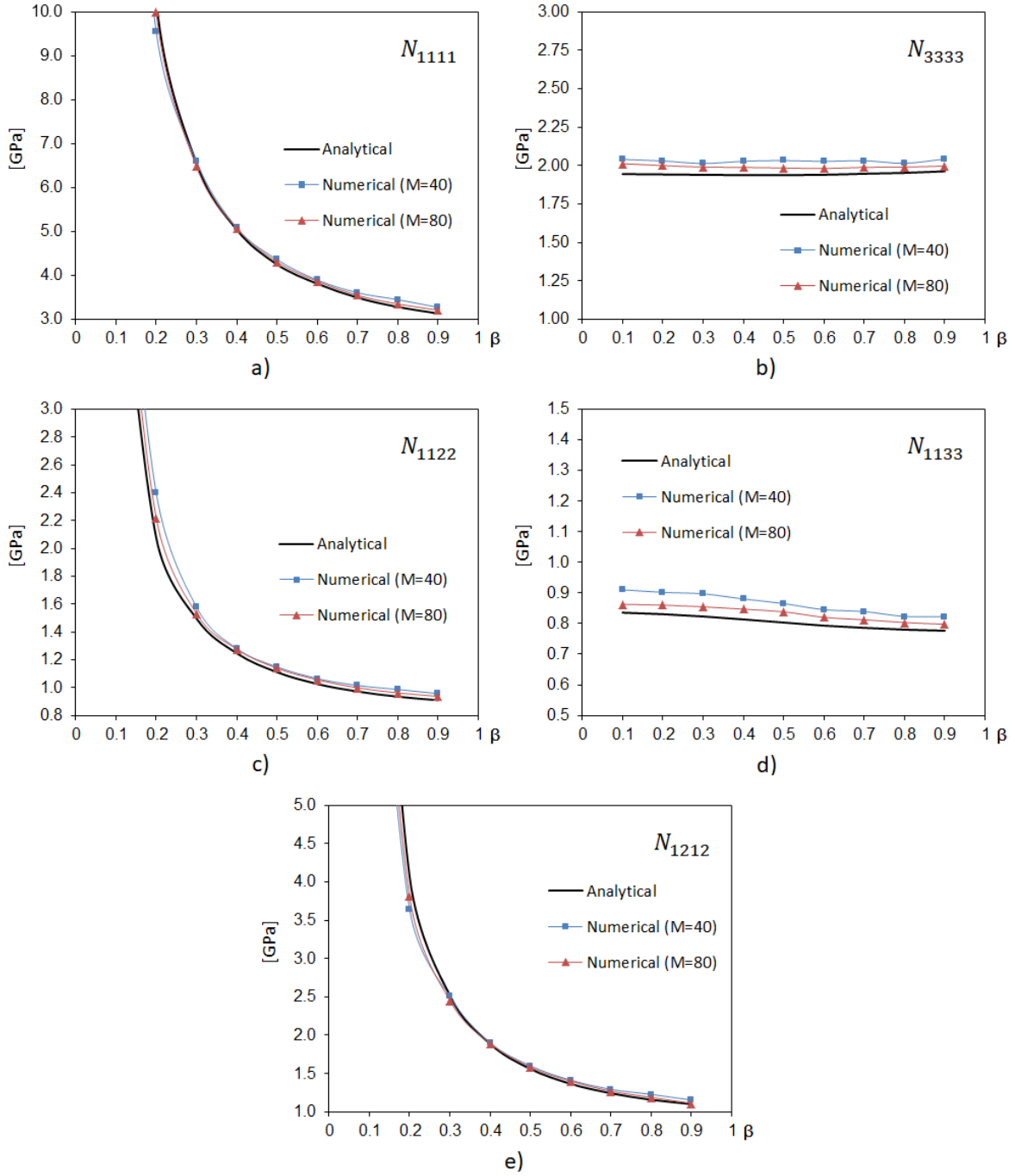


Figure 8. Components of the stiffness contribution tensor of a toroidal inclusion a) N_{1111} , b) N_{3333} , c) N_{1122} , d) N_{1133} , e) N_{1212} as functions of the ratio β .

Similarly to the previous problems, the difference between the analytical and numerical solutions does not exceed 2.5% for $M = 80$ and 5% for $M = 40$. The calculation CPU times was about 25 minutes in the case $M = 80$ and 5 minutes in the case $M = 40$.

5.4. Pores of irregular shape.

In order to complete the validation procedure, we compared our predictions of property contribution tensors against the FEM results obtained by Drach et al. [40] for the case of “irregularly” shaped (non-ellipsoidal) pore. The shape was imported by using the original .stl file (Figure 13).

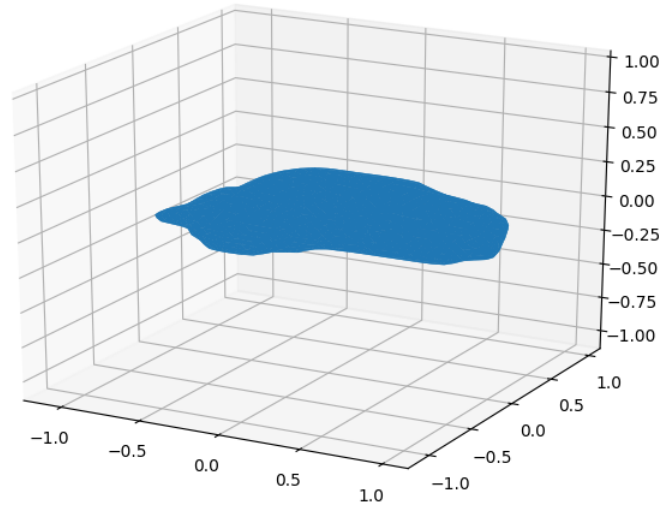


Figure 13. An irregular shape visualized by AMAT software.

The Young’s modulus of the matrix was assumed to be 1 GPa so that the results would correspond to the normalized results of Drach et al. [40] listed in Table 3 and the Poisson’s ratio was equal to 0.3. The results obtained by the AMAT software are given in Tables 1 and 2.

1.467	-0.400	-0.458	0.003	-0.063	-0.112
-0.400	2.196	-0.688	-0.025	0.016	-0.062
-0.458	-0.688	3.452	-0.028	-0.060	0.059
0.003	-0.025	-0.028	7.378	-0.198	-0.155
-0.063	0.016	-0.060	-0.198	6.332	-0.050
-0.112	-0.062	0.059	-0.155	-0.050	4.534

Table 1. Compliance contribution tensor of the irregularly shaped pore used by Drach et al. [40] calculated by using the AMAT software and $M = 80$. The results are given in 1/GPa.

1.438	-0.392	-0.446	0.003	-0.062	-0.107
-0.392	2.135	-0.664	-0.024	0.015	-0.060
-0.446	-0.664	3.361	-0.028	-0.058	0.055
0.003	-0.024	-0.028	7.069	-0.185	-0.147
-0.062	0.015	-0.058	-0.185	6.121	-0.049
-0.107	-0.060	0.055	-0.147	-0.049	4.416

Table 2. Compliance contribution tensor of the irregularly shaped pore used by Drach et al. [40] calculated by using the AMAT software and $M = 160$.

1.408	-0.383	-0.433	0.028	0.036	-0.146
-0.383	2.065	-0.635	-0.026	-0.020	-0.130
-0.433	-0.635	3.260	-0.076	-0.158	0.084
0.028	-0.026	-0.076	6.756	-0.084	-0.140
0.036	-0.020	-0.158	-0.084	5.912	-0.024
-0.146	-0.130	0.084	-0.140	-0.024	4.288

Table 3. The compliance contribution tensor of the irregularly shaped pore calculated by Drach et al. [40]. The results are given in 1/GPa.

One may note that the difference between the principal components of the compliance contribution tensor calculated by FEM and the AMAT software is about 2-3% in the case of $M = 160$ and 4-6% for $M = 80$. Meanwhile, the calculation CPU times were about 1 hour and 15 minutes, respectively.

6. Concluding remarks.

We have developed an open access program named AMAT to calculate compliance and stiffness contribution tensors for inhomogeneities of arbitrary shape that may be described either by explicit equation or graphically using .stl file. The software was tested and runs reliably on Windows operating systems, no additional installations were required. Calculations are done using mesh free numerical method based on a class of Gaussian approximating functions developed by Kanaun [46], [47]. Compliance and stiffness contribution constitute the basic building block for calculation of the overall elastic properties of heterogeneous materials (Kachanov and Sevostianov [50]). Presently, only limited number of results is available for 3-D inhomogeneities of irregular shape which complicates the procedure of evaluation of the effective elastic properties of materials containing non-ellipsoidal inhomogeneities. Our program fills this gap and simplifies the homogenization technique for materials with irregular microstructure. We illustrated the application of the program on several examples. First, to

illustrate the accuracy of the code, we considered spheroidal inhomogeneity and elliptical crack for which explicit analytical solutions are known. Then, we considered toroidal inhomogeneity and compared the result with analytical solution of Krasnitskii et al. [18] for a rigid torus obtained in the form of infinite series. Finally, we showed how the program can be applied to inhomogeneities of irregular shape described graphically. In its present version, the program works with isotropic materials only. In the future, we plan to extend the program to calculate property contribution tensors of inhomogeneities embedded in anisotropic matrices (Kanaun [58]), to extend the code to (simpler) conductivity problem (Kanaun and Babaii [59]), and to develop a block for calculation of the overall properties of inhomogeneous materials using various homogenization techniques (Markov and Kanaun [60], [61]). The latest version of the software can be downloaded from the website of NMSU Center for Micromechanics <https://centerformichromechanics.nmsu.edu>.

Acknowledgement.

IS acknowledges financial support of National Aeronautics and Space Administration (NASA) Cooperative Agreement NNX15AL51H.

References.

- [1] H. Horii and S. Nemat-Nasser, "Overall moduli of solids with microcracks: Load-induced anisotropy," *J. Mech. Phys. Solids*, vol. 31, no. 2, pp. 155–171, 1983.
- [2] S. Nemat-Nasser and M. Hori, *Micromechanics: Overall Properties of Heterogeneous Solid*. Elsevier Science Publishers, 1993.
- [3] M. Kachanov, I. Tsukrov, and B. Shafiro, "Effective Moduli of Solids With Cavities of Various Shapes," *Appl. Mech. Rev.*, vol. 47, no. 1S, p. S151, 1994.
- [4] I. Sevostianov and M. Kachanov, "Compliance tensors of ellipsoidal inclusions," *Int. J. Fract.*, vol. 96, no. 1, pp. 3–7, 1999.
- [5] I. Sevostianov and M. Kachanov, "On elastic compliances of irregularly shaped cracks," *Int. J. Fract.*, vol. 114, no. 3, pp. 245–257, 2002.

- [6] I. Sevostianov, N. Yilmaz, V. Kushch, and V. Levin, “Effective elastic properties of matrix composites with transversely-isotropic phases,” *Int. J. Solids Struct.*, vol. 42, no. 2, pp. 455–476, 2005.
- [7] V. I. Kushch and I. Sevostianov, “Effective elastic moduli of a particulate composite in terms of the dipole moments and property contribution tensors,” *Int. J. Solids Struct.*, vol. 53, pp. 1–11, 2015.
- [8] J. D. Eshelby, “The Determination of the Elastic Field of an Ellipsoidal Inclusion, and Related Problems,” *Proc. R. Soc. A Math. Phys. Eng. Sci.*, vol. 241, no. 1226, pp. 376–396, 1957.
- [9] J. D. Eshelby, “Elastic inclusions and inhomogeneities,” *Prog. Solid Mech.*, vol. 2, pp. 89–140, 1961.
- [10] T. Mura, *Micromechanics of defects in solids*, 3rd ed. Dordrecht: Springer Netherlands, 1987.
- [11] R. W. Zimmerman, “Compressibility of Two-Dimensional Cavities of Various Shapes,” *J. Appl. Mech.*, vol. 53, no. 3, p. 500, 1986.
- [12] I. Jasiuk, J. Chen, and M. Thorpe, “Elastic moduli of two dimensional materials with polygonal and elliptical holes,” *Appl. Mech. Rev.*, vol. 47, no. 1, pp. 18–28, 1994.
- [13] I. Tsukrov and J. Novak, “Effective elastic properties of solids with defects of irregular shapes,” *Int. J. Solids Struct.*, vol. 39, no. 6, pp. 1539–1555, Mar. 2002.
- [14] I. Tsukrov and J. Novak, “Effective elastic properties of solids with two-dimensional inclusions of irregular shapes,” *Int. J. Solids Struct.*, vol. 41, no. 24–25, pp. 6905–6924, Dec. 2004.
- [15] T. C. Ekneligoda and R. W. Zimmerman, “Compressibility of two-dimensional pores having n-fold axes of symmetry,” *Proc. R. Soc. A Math. Phys. Eng. Sci.*, vol. 462, no. 2071, pp. 1933–1947, Jul. 2006.
- [16] T. C. Ekneligoda and R. W. Zimmerman, “Shear compliance of two-dimensional pores

- possessing N-fold axis of rotational symmetry,” *Proc. R. Soc. A Math. Phys. Eng. Sci.*, vol. 464, no. 2091, pp. 759–775, Mar. 2008.
- [17] I. Argatov and I. Sevostianov, “Rigid toroidal inhomogeneity in an elastic medium,” *Int. J. Eng. Sci.*, vol. 49, no. 1, pp. 61–74, 2011.
- [18] S. Krasnitskii, A. Trofimov, E. Radi, and I. Sevostianov, “Effect of a rigid toroidal inhomogeneity on the elastic properties of a composite,” *Math. Mech. Solids*, vol. 24, no. 4, pp. 1129–1146, 2019.
- [19] B. Drach, I. Tsukrov, T. S. Gross, S. Dietrich, K. Weidenmann, R. Piat, and T. Böhlke, “Numerical modeling of carbon/carbon composites with nanotextured matrix and 3D pores of irregular shapes,” *Int. J. Solids Struct.*, vol. 48, no. 18, pp. 2447–2457, 2011.
- [20] I. Sevostianov, M. Kachanov, and T. Zohdi, “On computation of the compliance and stiffness contribution tensors of non ellipsoidal inhomogeneities,” *Int. J. Solids Struct.*, vol. 45, no. 16, pp. 4375–4383, 2008.
- [21] I. Sevostianov and A. Giraud, “On the compliance contribution tensor for a concave superspherical pore,” *Int. J. Fract.*, vol. 177, no. 2, pp. 199–206, 2012.
- [22] F. Chen, I. Sevostianov, A. Giraud, and D. Grgic, “Evaluation of the effective elastic and conductive properties of a material containing concave pores,” *Int. J. Eng. Sci.*, vol. 97, pp. 60–68, 2015.
- [23] I. Sevostianov, F. Chen, A. Giraud, and D. Grgic, “Compliance and resistivity contribution tensors of axisymmetric concave pores,” *Int. J. Eng. Sci.*, vol. 101, pp. 14–28, 2016.
- [24] F. Chen, I. Sevostianov, A. Giraud, and D. Grgic, “Combined effect of pores concavity and aspect ratio on the elastic properties of a porous material,” *Int. J. Solids Struct.*, vol. 134, pp. 161–172, Mar. 2018.
- [25] A. Trofimov, A. Markov, S. G. Abaimov, I. Akhatov, and I. Sevostianov, “Overall elastic properties of a material containing inhomogeneities of concave shape,” *Int. J. Eng. Sci.*, vol. 132, pp. 30–44, 2018.

- [26] A. Markov, A. Trofimov, S. Abaimov, and I. Akhatov, "On the applicability of replacement relations to tetrahedron-like inhomogeneities," *Int. J. Solids Struct.*, vol. 167, pp. 1–13, Aug. 2019.
- [27] A. Trofimov, B. Drach, and I. Sevostianov, "Effective elastic properties of composites with particles of polyhedral shapes," *Int. J. Solids Struct.*, vol. 120, pp. 157–170, Aug. 2017.
- [28] A. Trofimov and I. Sevostianov, "The effect of waviness of a helical inhomogeneity on its stiffness- and conductivity contribution tensors," *Int. J. Eng. Sci.*, vol. 116, 2017.
- [29] A. Trofimov, S. Abaimov, I. Akhatov, and I. Sevostianov, "Effect of elastic contrast on the contribution of helical fibers into overall stiffness of a composites," *Int. J. Eng. Sci.*, vol. 120, pp. 31–50, Nov. 2017.
- [30] V. I. Fabrikant, *Applications of potential theory in mechanics : a selection of new results*. Dordrecht: Boston : Kluwer Academic Publishers, 1989.
- [31] V. Grechka, I. Vasconcelos, and M. Kachanov, "The influence of crack shape on the effective elasticity of fractured rocks," *Geophysics*, vol. 71, no. 5, pp. D153–D160, Sep. 2006.
- [32] M. E. Mear, I. Sevostianov, and M. Kachanov, "Elastic compliances of non-flat cracks," *Int. J. Solids Struct.*, vol. 44, no. 20, pp. 6412–6427, Oct. 2007.
- [33] M. Kachanov and I. Sevostianov, "Rice's Internal Variables Formalism and Its Implications for the Elastic and Conductive Properties of Cracked Materials, and for the Attempts to Relate Strength to Stiffness," *J. Appl. Mech.*, vol. 79, no. 3, p. 031002, 2012.
- [34] A. Trofimov, B. Drach, M. Kachanov, and I. Sevostianov, "Effect of a partial contact between the crack faces on its contribution to overall material compliance and resistivity," *Int. J. Solids Struct.*, vol. 108, pp. 289–297, Mar. 2017.
- [35] A. Markov, S. Abaimov, I. Sevostianov, M. Kachanov, S. Kanaun, and I. Akhatov, "The effect of multiple contacts between crack faces on crack contribution to the effective elastic properties," *Int. J. Solids Struct.*, Dec. 2018.

- [36] A. Markov, A. Trofimov, and I. Sevostianov, "Effect of non-planar cracks with islands of contact on the elastic properties of materials," *Int. J. Solids Struct.*, vol. 191–192, pp. 307–314, May 2020.
- [37] A. Rasool and H. J. Böhm, "Effects of particle shape on the macroscopic and microscopic linear behaviors of particle reinforced composites," *Int. J. Eng. Sci.*, vol. 58, pp. 21–34, Sep. 2012.
- [38] H. J. Böhm and A. Rasool, "Effects of particle shape on the thermoelastoplastic behavior of particle reinforced composites," *Int. J. Solids Struct.*, vol. 87, pp. 90–101, 2016.
- [39] B. Drach, A. Drach, and I. Tsukrov, "Prediction of the effective elastic moduli of materials with irregularly-shaped pores based on the pore projected areas," *Int. J. Solids Struct.*, vol. 51, no. 14, pp. 2687–2695, 2014.
- [40] B. Drach, I. Tsukrov, and A. Trofimov, "Comparison of full field and single pore approaches to homogenization of linearly elastic materials with pores of regular and irregular shapes," *Int. J. Solids Struct.*, vol. 96, pp. 48–63, Oct. 2016.
- [41] A. P. Roberts and E. J. Garboczi, "Elastic properties of a tungsten–silver composite by reconstruction and computation," *J. Mech. Phys. Solids*, vol. 47, no. 10, pp. 2029–2055, Oct. 1999.
- [42] A. P. Roberts and E. J. Garboczi, "Computation of the linear elastic properties of random porous materials with a wide variety of microstructure," *Proc. R. Soc. London. Ser. A Math. Phys. Eng. Sci.*, vol. 458, no. 2021, pp. 1033–1054, May 2002.
- [43] C. H. Arns, M. A. Knackstedt, W. V. Pinczewski, and E. J. Garboczi, "Computation of linear elastic properties from microtomographic images: Methodology and agreement between theory and experiment," *Geophysics*, vol. 67, no. 5, pp. 1396–1405, Sep. 2002.
- [44] E. J. Garboczi and J. F. Douglas, "Elastic moduli of composites containing a low concentration of complex-shaped particles having a general property contrast with the matrix," *Mech. Mater.*, vol. 51, pp. 53–65, 2012.
- [45] V. Maz'ya and G. Schmidt, *Approximate approximation. American mathematical society.*

Providence: Mathematical Surveys and Monographs, 2007.

- [46] S. Kanaun, “Fast Calculation of Elastic Fields in a Homogeneous Medium with Isolated Heterogeneous Inclusions,” *Int. J. Multiscale Comput. Eng.*, vol. 7, no. 4, pp. 263–276, 2009.
- [47] S. K. Kanaun, “Fast Solution of 3D-Elasticity Problem of a Planar Crack of Arbitrary Shape,” *Int. J. Fract.*, vol. 148, no. 4, pp. 435–442, Dec. 2007.
- [48] S. Kanaun and A. Markov, “Stress fields in 3D-elastic material containing multiple interacting cracks of arbitrary shapes: Efficient calculation,” *Int. J. Eng. Sci.*, vol. 75, 2014.
- [49] S. Babaii Kocheksaraii, “Effective conductivity of matrix composites and foam materials by self-consistent field method using commercial FEA software,” *Int. J. Eng. Sci.*, vol. 98, pp. 110–115, 2016.
- [50] M. Kachanov and I. Sevostianov, *Micromechanics of Materials, with Applications*, 1st ed. Springer International Publishing, 2018.
- [51] R. Hill, “Elastic Properties of Reinforced Solids: Some Theoretical Principles,” *Journal of the Mechanics and Physics of Solids*, vol. 11, pp. 357–372, 1963.
- [52] Z. Hashin, “Analysis of Composite Materials—A Survey,” *J. Appl. Mech.*, vol. 50, no. 3, p. 481, 1983.
- [53] S. Kanaun and V. Levin, *Self-consistent methods for composites I*. Dordrecht: Springer., 2008.
- [54] S. Kanaun, “Elastic problem for 3D-anisotropic medium with a crack.,” *Appl. Math. Mech.*, vol. 45, pp. 361–370, 1981.
- [55] I. Kunin, *Elastic Media with Microstructure II*, 1st ed. Springer Berlin Heidelberg, 1983.
- [56] S. Kanaun and E. Pervago, “Combining self-consistent and numerical methods for the calculation of elastic fields and effective properties of 3D-matrix composites with periodic and random microstructures,” *Int. J. Eng. Sci.*, vol. 49, no. 5, pp. 420–442, May 2011.

- [57] S. Kanaun, A. Markov, and S. Babaii, “An efficient numerical method for the solution of the second boundary value problem of elasticity for 3D-bodies with cracks,” *Int. J. Fract.*, vol. 183, no. 2, pp. 169–186, Oct. 2013.
- [58] S. Kanaun, “Fast solution of the elasticity problem for a planar crack of arbitrary shape in 3D-anisotropic medium,” *Int. J. Eng. Sci.*, vol. 47, no. 2, pp. 284–293, 2009.
- [59] S. K. Kanaun and S. B. Kocheckaraii, “Effective conductive and dielectric properties of matrix composites with inclusions of arbitrary shapes,” *Int. J. Eng. Sci.*, vol. 46, no. 2, pp. 147–163, Feb. 2008.
- [60] A. Markov and S. Kanaun, “An efficient homogenization method for elastic media with multiple cracks,” *Int. J. Eng. Sci.*, vol. 82, 2014.
- [61] A. Markov and S. Kanaun, “Interactions of cracks and inclusions in homogeneous elastic media,” *Int. J. Fract.*, vol. 206, no. 1, 2017.